Full Spectroscopic Tip-Enhanced Raman Imaging of Single Nanotapes Formed from β-Amyloid(1−40) Peptide Fragments
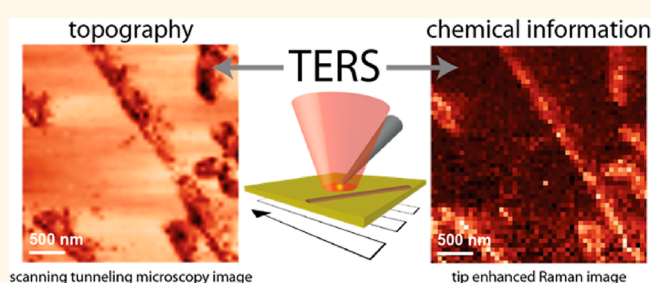
Melissa Paulite,[‡,§] Carolin Blum,[†,§] Thomas Schmid,[†] Lothar Opilik,[†] Klaus Eyer,[†] Gilbert C. Walker,[‡] and Renato Zenobi[†,*]

[†]Department of Chemistry and Applied Biosciences, Laboratory of Organic Chemistry, ETH Zurich, 8093 Zurich, Switzerland and [‡]Department of Chemistry, Lash Miller Chemical Laboratories, University of Toronto, Toronto, ON, Canada M5S 3H6. [§]These authors contributed equally to this work.

ABSTRACT This study demonstrates that spectral fingerprint patterns for a weakly scattering biological sample can be obtained reproducibly and reliably with tip-enhanced Raman spectroscopy (TERS) that correspond well with the conventional confocal Raman spectra collected for the bulk substance. These provided the basis for obtaining TERS images of individual self-assembled peptide nanotapes using an automated, objective procedure that correlate with the simultaneously obtained scanning tunneling microscopy (STM)

images. TERS and STM images (64×64 pixels, $3 \times 3 \, \mu m^2$) of peptide nanotapes are presented that rely on marker bands in the Raman fingerprint region. Full spectroscopic information in every pixel was obtained, allowing post-processing of data and identification of species of interest. Experimentally, the "gap-mode" TERS configuration was used with a solid metal (Ag) tip in feedback with a metal substrate (Au). Confocal Raman data of bulk nanotapes, TERS point measurements with longer acquisition time, atomic force microscopy images, and an infrared absorption spectrum of bulk nanotapes were recorded for comparison. It is shown that the unique combination of topographic and spectroscopic data that TERS imaging provides reveals differences between the STM and TERS images, for example, nanotapes that are only weakly visible in the STM images, a coverage of the surface with an unknown substance, and the identification of a patch as a protein assembly that could not be unambiguously assigned based on the STM image alone.

KEYWORDS: tip-enhanced Raman spectroscopy · TERS · β-amyloid nanotapes · imaging · marker band

Tip-enhanced Raman spectroscopy is a surface-sensitive analytical near-field technique that combines the high spatial resolution achievable in scanning probe microscopy with the chemical information provided by Raman spectroscopy.[1] A diffraction-limited laser beam is focused onto the end of a very sharp metal-coated or solid metal tip that is in close proximity to the sample of interest. A confined and enhanced electromagnetic field at the tip apex leads to a strong enhancement of the Raman signal of the molecules in the vicinity of the tip end.[2] Since the localization of the enhanced electromagnetic field is dependent on the dimensions of the tip end, the spatial resolution is no longer determined by the diffraction-limited laser focus but by the size and shape of the tip apex.[3] Therefore,

it is possible to obtain a spatial resolution well below the optical diffraction limit, in the range of 10−15 nm.[4,5] TERS has the potential to investigate biological nanostructures since the additional Raman signal enhancement allows one to probe weakly scattering biological molecules. Additionally, the spatial resolution that TERS can achieve is in the size range of numerous biological entities with nanoscale dimensions.

Rational design of biological nanostructures through the self-assembly of molecules such as proteins[6,7] and peptides[8−10] has been widely investigated. Utilizing these molecules for nanoengineering purposes attracts considerable interest due to their straightforward synthesis, biocompatibility, and ease of chemical and structural modification.[11−15] As the major cause for peptide self-assembly, strong

evidence points to noncovalent forces such as van der Waals interactions, hydrogen bonding, $\pi-\pi$ stacking, and electrostatic interactions.[7,16,17]

A well-characterized peptide that self-assembles into nanostructures is the Aβ(16−22) sequence (Ac-KLVFFAE-NH$_2$) that is part of the β-amyloid peptide, which is a major constituent in amyloid plaques associated with Alzheimer's disease.[15] It has been demonstrated that the Aβ(16−22) peptide can form amyloid fibrils *in vitro* and is believed to play a key role in the full Aβ(1−40) peptide's amyloid fibril conformation.[12,15,18] Interestingly, it has been demonstrated that, under different pH conditions and with various termini of the peptide, very different morphological nanostructures, such as amyloid fibrils, nanotapes, and hollow nanotubes, are obtained.[18−21]

In this study, the first TERS *images* of biological nanotapes (synthesized from the Aβ(16−22) peptide) based on signals in the Raman fingerprint region (400−1500 cm^{-1}) are shown together with simultaneously obtained STM images. So far, only two other TERS imaging studies on biological samples have been published, namely, on lipid domains[22] and on a biotin-labeled Au nanoparticle bound to a streptavidin-functionalized surface.[23] The study on lipid domains focused on the high wavenumber region (2000−3000 cm^{-1}), and the study of the biotin-labeled Au nanoparticle used the special condition of a hot spot between the tip and a single particle.

Other TERS studies of biological nanostructures do not show images but rely on single-point measurements or line scans only.[4,24,25] Previous TERS measurements on amyloid fibrils,[26] collagen I fibrils,[27] and insulin fibrils[28,29] only showed TER spectra collected from individual positions. Unfortunately, these TER spectra are often inconclusive: the spectral fingerprint patterns that are shown differ significantly from laboratory to laboratory, and even within the same experimental series. In contrast, the results presented here demonstrate that a highly reproducible TER spectral fingerprint is obtained that corresponds well with the confocal Raman spectrum collected of bulk nanotapes. No fluctuating band pattern is observed (as would be observed when contamination is present or decomposition occurs). It is, in fact, precisely this reproducibility in the TER spectra that allows us to generate reliable TERS images of the nanotapes, which, moreover, correlate well with the simultaneously obtained STM images. In addition, the evaluation of the data is performed using a straightforward, automated, and unbiased method, that is, by always integrating over the same spectral range, without relying on a subjective individual assignment of TER spectra by the researcher or a complex mathematical analysis. This is only possible if the fingerprint pattern of the TER spectra is reproducible.

It is shown that obtaining a STM and a TERS image simultaneously allows one to (a) identify structural differences within the studied nanotapes, (b) detect nanotapes that are not clearly visible in the STM image, (c) unveil the coverage of the surface with an unknown substance that could only be identified based on the full spectrum TERS image, and (d) identify a structure that could not be unambiguously assigned in the STM image as a protein assembly. Interestingly, this work also confirms that the amide I mode is not observed in gap-mode STM-TERS, as shown before.[30] The assignment of secondary structure of the amyloid nanotapes, which is usually based on the band position of the amide I mode, was therefore not possible. However, the TERS fingerprint images shown in this study illustrate the potential of TERS as a reliable, reproducible imaging technique for weakly scattering biological samples that simultaneously yields topographical and chemical information with nanoscale resolution.

RESULTS AND DISCUSSION

An Abeta(16−22) peptide solution was deposited onto an ultraflat Au substrate (that was prepared by a template stripping method)[31] and characterized using atomic force microscopy (AFM), as shown in Figure 1. An acetylated N-terminus and an amidated C-terminus of the peptide were chosen because they mimic the native charge state of the amyloid protein.[15] According to the AFM images collected, the nanotapes have a ribbon-like, flat morphology and are up to several micrometers long. Although there are some nanotapes observed that are wider and thinner, the majority of the nanotapes (see Figure 1a) have the same height and width. Cross section analysis of 21 nanotapes in two different AFM images (see Figures S1 and S2 in the Supporting Information) reveals that the physical dimensions of the nanotapes are 5.4 $\pm$ 0.9 nm in height and 203.7 $\pm$ 18.0 nm in width.

The morphology and dispersity of the nanotapes used in this study are very similar to the nanotapes synthesized by Cui *et al.* using alkylated peptide amphiphiles[10] and by Tao *et al.* using the same peptide sequence utilized in the present work.[19] In both cases, the authors state that the peptides may arrange in stacked bilayers within the nanotapes (see Figure 2). Depending on the peptide concentration and the pH of the solution, the lateral width of the nanotapes varies but has been shown to be consistent within the same solution.[10,19]

The length of an extended Aβ(16−22) peptide is calculated to be approximately 2.5 nm (where the distance between adjacent amino acid residues is approximately 360 pm). Therefore, the peptide bilayer thickness is calculated to be approximately 5.0 nm (2 $\times$ 2.5 nm), which is in agreement with the height of the analyzed nanotapes (5.4 $\pm$ 0.9 nm), as derived from the AFM images. This provides strong evidence that the nanotapes are composed of peptide bilayers. This is
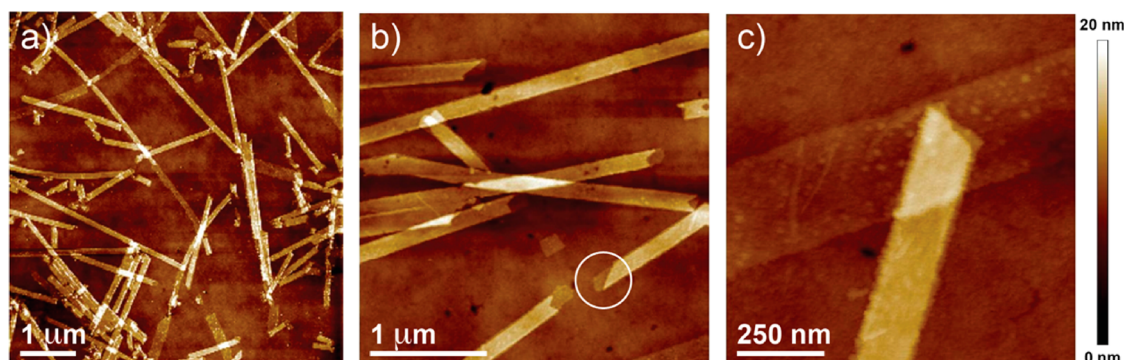
Figure 1. Representative AFM height images of individual nanotapes on a gold surface. Cross section analysis of 21 nanotapes (see Figures S1 and S2 in the Supporting Information) reveals that they are 5.4 ± 0.9 nm in height and 203.7 ± 18.0 nm in width. (a,b) Most of the nanotapes are in the same width and height range. The white circle in (b) highlights a peptide monolayer fragment at the end of a broken nanotape. (c) Two nanotape pieces, with the wide one most likely consisting of a peptide monolayer and the narrow one of a peptide bilayer.
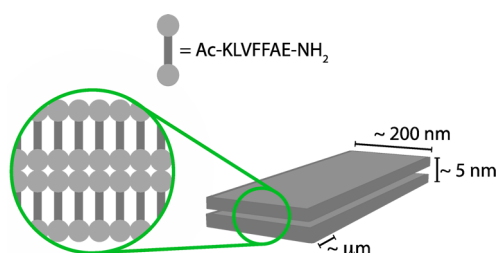

Figure 2. Illustration of the proposed stacked bilayer arrangement of the Aβ(16−22) peptide within the nanotape structure.
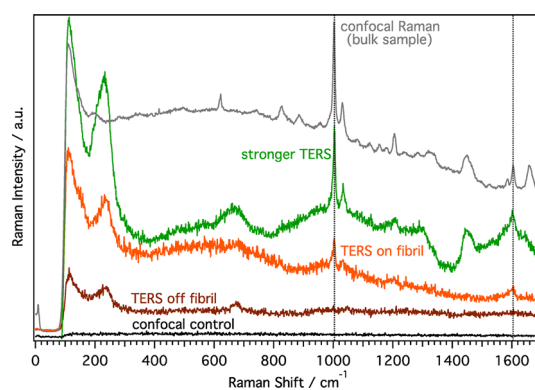

Figure 3. Orange: TER spectrum from an individual nanotape. Brown: TER spectrum from a position next to a nanotape. Both spectra are extracted from the full spectrum map (acquisition time 1 s/pixel, 2 mW incident power) of the TERS images shown in Figure 4b,c. Black: Representative confocal Raman spectrum of the nanotape sample that was extracted from the full spectral map that the images in Figure S3 are based on. Gray: Confocal Raman spectrum of the bulk nanotapes (acquisition time 30 min, 2 mW incident power). Green: More intense TER spectrum (additional point measurement) on a nanotape (acquisition time 2 min, 240 μW incident power).

also supported by the fact that, in the AFM image in Figure 1b, fibrils with broken edges exhibit features with approximately half the thickness (2.4 nm) of the intact fibril that could be leftover monolayer parts (white circle) and nanotapes are observed that are wider but only half as tall (see Figure 1c). Similar to the study of Tao *et al.*,[19] the self-assembly of flat nanotapes instead of nanofibrils can be explained by a fine balance between lateral adhesion (lateral interactions between adjacent peptide chains due to favorable side chain interactions, hydrophobic interactions, *etc.*) *versus* the intrinsic property of β-sheets to twist due to their chirality.[32−34] Tao *et al.* state that the widths of their nanotapes were on the order of 80 nm and increased as the pH of the solution became basic. In our case, the widths of the nanotapes measured are more than twice as wide as observed by Tao *et al.*, which could be attributed to greater lateral interactions (see next section) within our sample as well as different pH conditions present within our peptide solution.

The FTIR spectrum of the mature solution (containing nanotapes with ribbon-like, flat morphology and lengths of up to several micrometers, as shown in Figure 1) in Figure S4 in the Supporting Information shows two peaks at 1621 and 1690 cm^{-1}, with the low wavenumber peak having greater amplitude than the high wavenumber peak.[35] This indicates the likely presence of an antiparallel

β-sheet next to a parallel β-sheet secondary structure. We hypothesize that the nanotape solution contains a mixture of nanotapes with parallel and antiparallel β-sheet secondary structure. As described by Tao *et al.*, the formation of a peptide bilayer within the nanotape structure is possible when the peptides arrange in a parallel β-sheet manner. In this way, the charged headgroup (positively or negatively charged, depending on the pH) would point to the outside of the nanotape into a polar solvent, while the uncharged end of the peptide would point inward, similar to the behavior of surfactants. However, we also observe the presence of nanotapes that are about a monolayer thick, as seen in Figure 1c. In this case, an antiparallel arrangement of the peptides is possible for the Aβ(16−22) amyloid fibrils, as described by Balbach *et al.*[15] They suggest a favored electrostatic interaction between C- and N-termini of neighboring

molecules as a possible driving force for the formation of antiparallel β-sheet stacking. Further evidence for the presence of β-sheets is also observed in the confocal Raman spectrum of the nanotape sample (lyophilized from a mature solution and named "bulk sample" (gray spectrum in Figure 3)), in which a peak at 1660 cm^{-1} in the amide I region indicates β-sheet secondary structures within the nanotapes.[36] The presence of the β-sheets could further promote the stronger lateral interactions that were described previously. However, a detailed explanation of the molecular structure is still being pursued.

Tip-enhanced Raman spectroscopy in the gap-mode configuration was used to investigate the nanotapes due to the following reasons: first, their size is well below the optical diffraction limit. The high lateral resolution of TERS offers the opportunity to probe individual nanotapes.[1] Second, it is possible to simultaneously obtain topographical information that can be related to the spectroscopic information extracted from the TER spectra. Finally, these tapes are, as many other biological materials, very weak Raman scatterers. The strongly confined and enhanced electromagnetic field at the apex of the TERS tip leads to an enhancement of the Raman signal of a factor of up to 10^5 (AFM-TERS) that enables probing of such very weak Raman scatterers.[1,24,37] Gap-mode STM-TERS with its special geometry of a metal tip in feedback with a conducting metal surface is known to provide even higher enhancement factors of up to 10^7.[3] Since it is crucial to keep the acquisition times short when imaging biological substrates (in order to avoid sample damage due to laser-induced decomposition and/or sample drift), the very strong electromagnetic enhancement reached by gap-mode STM-TERS is highly beneficial for imaging experiments. Since the nanotapes used in this study are only 3–5 nm in height, the maintenance of the tunneling current feedback between the Ag tip and the Au substrate was possible. Therefore, the huge enhancement effects of gap-mode STM-TERS could be exploited in this study to obtain fingerprint TERS images of biological nanotapes. However, in the gap-mode STM-TERS configuration, it was previously shown that the amide I mode is not observed, and therefore, information about the secondary structure of the protein or peptide is not available.[30]

For comparison with the TERS data, a confocal Raman spectrum of the bulk nanotape sample was collected (30 min, 2 mW; see Figure 3, gray spectrum). The observed spectral band pattern is consistent with the amino acid sequence of the Aβ(1−40) peptide fragment, Ac-KLVFFAE-NH$_2$ (see also Table S1 in the Supporting Information): aromatic ring breathing mode at 1004 cm^{-1}, in-plane ring C−H bending mode at 1031 cm^{-1}, C$_6$H$_5$−C vibration at 1206 cm^{-1}, CH deformation modes and amide III around 1300 cm^{-1}, CH$_2$ scissoring modes at 1450 cm^{-1}, ring C−C

vibrations at 1604 cm^{-1}, and the amide I mode at 1660 cm^{-1}.[38−44] In general, the aromatic modes of the phenyl rings dominate the confocal Raman spectrum of the nanotapes due to the higher Raman cross section of the aromatic rings.[39,42,45]

A first TER spectrum of the nanotapes was collected using a point measurement (2 min acquisition time, laser power reduced to 240 μW to avoid sample damage) represented by the green spectrum in Figure 3. The aim of this experiment was to obtain a spectrum with a high signal-to-noise ratio since this TER spectrum is easier to compare to the bulk confocal Raman data than the TER spectra from the full spectral map due to a minimized acquisition time per pixel and therefore a smaller signal-to-noise ratio. Note that the TER spectrum has an inelastic scattering background that is not as uniform as the background in the confocal Raman spectrum. This is due to the fact that none of the spectra shown have been background corrected. The main factors that might contribute to this background can be found in ref 30. More importantly, what is already known about how TERS compares to confocal Raman spectroscopy of nonresonant weakly scattering biological molecules is confirmed when comparing the TER spectrum (green spectrum, Figure 3) of the nanotapes with their bulk confocal Raman spectrum (gray spectrum, Figure 3): the band positions match, although in TERS, fewer bands are present; the intensity ratios of the bands change dramatically, and aromatic modes dominate the fingerprint pattern.[30,31] Note that this is *not* due to a small signal-to-noise ratio since the aromatic modes at 1004 and 1600 cm^{-1} as well as the CH$_2$ mode at 1450 cm^{-1} have the same ratio as is observed in the confocal bulk Raman spectrum. A possible reason for the absence of certain modes may have to do with the special gap-mode STM-TERS configuration used that causes a strictly perpendicular orientation of the electromagnetic field lines with respect to the surface, which was discussed previously.[30] The characteristic bands in the TER spectrum in Figure 3 are as follows: the aromatic ring breathing mode at 1004 cm^{-1}, an in-plane ring C−H bending mode at 1031 cm^{-1}, the phenyl−C stretching mode at 1206 cm^{-1}, CH$_2$ scissoring modes at 1450 cm^{-1}, and the ring C−C vibrations at 1604 cm^{-1}. The TER spectrum is—like the confocal spectrum—dominated by the aromatic modes.

Figure 4 shows the results of the TERS imaging experiment on the nanotapes deposited on a template-stripped Au substrate. For each pixel of the image, a full TER spectrum and the STM height information were obtained simultaneously. Therefore, it was not necessary that one knows *a priori* which spectral feature will be important or which marker band is going to be used for generating an image, as the full spectra are available after the experiment.

Figure 4a shows the STM height image of the nanotapes (brighter pixel indicates the presence of a

taller feature). The lateral dimensions of the nanotapes displayed in Figure 4 are similar to the dimensions of the nanotapes deduced earlier from the AFM measurements (Figure 1). Note that the nanotapes appear with a negative (dark) contrast in the STM image, implying that they should be *deeper* than the Au substrate. This effect is already known from the STM literature: a STM tip that is not perfectly sharp will be positioned at a larger distance to the sample (we surmise that, in this study, the height of the STM tip relative to the substrate is larger than the height of the nanotapes) compared to a very sharp tip (same measurement parameters).[46] Due to this effect, there is no mechanical contact between the nanotapes and the Ag tip since they are sufficiently separated. Additionally, biological samples are, in general, less conductive than the air between the Ag tip and the Au substrate.[47] Therefore, the tunnel current between the STM tip and the Au substrate is lower when the tip crosses a nanotape. Since constant current mode was the STM modality used, the feedback triggers the nanotape stage to move *closer* to the sample in order to achieve the same tunnel current used when the Ag tip is placed above the metal substrate. This is the reason why a negative (dark) contrast in the STM image of the nanotapes is observed.

Note that if there were mechanical contact between the STM tip and the nanotapes, the tip would most likely have become contaminated. This would have been obvious in the remaining part of the TER measurement: the observation of contamination peaks in the TER spectra (a strong, varying band pattern that does not match the bulk confocal Raman spectrum of the nanotapes would be observed and/or two broad carbonaceous bands centered around 1350 and 1580 cm^{-1} would be present in the TER spectra, as described by Domke *et al.*),[48] the loss of correlation of the STM image with the TERS image, the same TERS signal observed within several scanning lines, and the loss of TERS enhancement are just a few examples of what would have been observed if contamination would have indeed taken place. In any case, we do not see evidence of significant contamination in our TERS images.

To generate an image of the nanotapes, the aromatic ring breathing mode at 1004 cm^{-1} was chosen as a marker band, as it was by far the dominant mode in the separately performed TER point measurement and the bulk confocal Raman measurement (Figure 3). Other TERS modes, such as the CH$_2$ scissoring mode at 1450 cm^{-1}, could have been used as a marker band, as well. However, much longer integration times per pixel would have been necessary to achieve a sufficient signal-to-noise ratio and would have caused additional difficulties such as sample drift, *etc.*, as mentioned above. The intensity of the aromatic ring breathing mode is color-coded (higher intensity/integral value is represented by brighter pixels) in the images shown in

Figure 4. The TERS image in Figure 4b is based on the peak area of the aromatic ring breathing mode (with respect to the background); the TERS image in Figure 4c is based on its peak maximum (with respect to the background). Figure 4b,c shows the same features even though different spectral evaluation methods (peak maximum *vs* peak integral) were used. Note that the images were created using an objective, computational evaluation method (always integrating the same peak (at the same position) in each TER spectrum) and are not based on a subjective, individual assignment of the spectra by the researcher. Therefore, the spectra must (and do) show the same spectral features in the same position (on the nanotapes *vs* next to them) reproducibly within the whole image. That the same spectroscopic answer (only differences in the intensity, not in the band pattern) is obtained on the nanotapes is understandable, as they consist of only one sort of molecule—the Aβ(16−22) peptide.

Two representative TER spectra of the full spectroscopic image are presented in Figure 3. The orange spectrum represents a spectrum collected on a nanotape, and the brown one represents a spectrum collected in the absence of a nanotape. The spectral fingerprint of the TER spectrum on the nanotape matches the TER spectrum obtained by the separate longer point measurement (green spectrum) and the confocal Raman spectrum of bulk nanotapes (gray spectrum) that have been discussed before.

Figure S3 (in the Supporting Information) shows a control image on the same region measured with confocal Raman spectroscopy (same laser power and acquisition time/pixel; color-coded image of the aromatic ring breathing mode) to ensure that the observed signal is only due to the enhancement of the tip and not due to a confocal background signal originating from the nanotapes. No spectral features belonging to nanotape structures are observed. A Raman spectrum extracted from this confocal full spectrum map is shown in Figure 3 (black spectrum) for comparison. A confocal Raman signal could also not be obtained in a longer point measurement on the same sample (10 min acquisition time, 1.7 mW laser power, data not shown). This control experiment emphasizes the importance of the huge enhancement effects of gap-mode STM-TERS. In the absence of these effects, it would not be possible to observe a Raman signal at all (with the parameters described before).

When comparing the STM image (Figure 4a) with the TERS images (Figure 4b,c), some differences and similarities can be found that also might be biologically relevant. Both TERS images show that the signal intensity of the aromatic ring breathing mode yields a spectroscopic image that correlates with the topographic image of the nanotapes obtained simultaneously by STM imaging. However, a closer look also reveals that the long nanotape from the top middle to the lower right is not continuous in the STM picture but
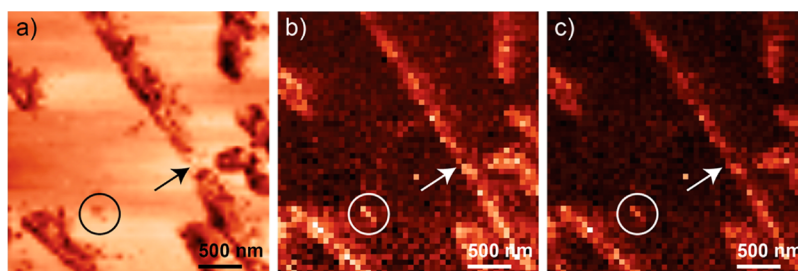
Figure 4. Simultaneously acquired (a) STM and (b,c) TERS (acquisition time 1 s/pixel, 2 mW incident power) images of individual nanotapes with 3×3 μm^2 scan size and 50×50 pixels. The color-coded TERS images display the intensity (high intensity is represented by a brighter pixel) of the aromatic ring breathing marker band (1004 cm^{-1}): (b) value of the peak integral, (c) peak maximum. The arrow and circle illustrate that areas weakly observed as a feature in the STM image can be identified as nanotape/peptide structures using TERS imaging.

continuous in the TERS image (arrow). Additionally, small structures on the surface (*e.g.*, highlighted by a circle) can clearly be identified as nanotape pieces or native peptide (as opposed to other substances that might be absorbed to the surface) because of the additional spectroscopic information available in the TERS images. Only TERS imaging allowed this information to be obtained.

Figure 5 demonstrates that similar TERS imaging measurements can be reproduced on another region of the sample. Figure 5a shows the STM image of the nanotapes in this area. Figure 5b shows the corresponding color-coded TERS image based on the integral value of the aromatic ring breathing marker band. Again, the TERS image of the nanotapes correlates with the STM topography image. Representative spectra extracted from the image can be seen in Figure 5d. When comparing the topography visible in the STM image with the TERS image, differences are clearly observed. Note in particular the following:

(i) As already shown for Figure 4, some structures that are visible in the TERS image are invisible in the corresponding STM image. The nanotape marked with a circle in Figure 5 shows approximately the same spectroscopic response as its two neighboring nanotapes, implying that these three nanotapes have similar chemical structures. However, in the STM image, the nanotape on the left cannot be observed at all but is observed very clearly in the TERS image. TERS is a surface-sensitive technique for which the signal enhancement decays rapidly within the first few nanometers distance from the tip apex.[49] We thus speculate that the enhanced signal mostly stems from the top layer of molecules on the nanotape. Therefore, the signal intensity in the TERS image will be similar for nanotapes of different height but similar chemical composition. In the STM image, however, different heights cause different contrasts. This could also be the explanation for the "missing" nanotape part in the STM image of Figure 4. Our interpretation is that the nanotape is thinner in this particular region and therefore is still visible with the same contrast in the TERS image but invisible in the STM image.

(ii) Nanotape 1 (see Figure 5) shows less contrast in the STM image than nanotape 2, implying that the latter structure is either thicker and/or less conductive, leading to the more negative (darker) contrast in the STM image. However, in the TERS image, the TER signal intensity of nanotape 1 is on average stronger than that of nanotape 2. At the moment, we can only speculate about the origin of the different intensities in the TERS image, but we believe that it is due to subtle, structural differences between the nanotapes. As discussed above, TERS signals should result mostly from the top layer of molecules and therefore should be similar for the nanotapes if there were no differences in their structure. Additionally, within the nanotapes, different signal intensities of the marker band are observed (different brightness of the pixels) in the TERS image. This is a strong hint for structural heterogeneities within the nanotapes.

(iii) Similar to what is observed in Figure 4, a piece that might not look like a nanotape structure (square in Figure 5) is safely identified as a piece of nanotape (or a structure containing the peptide) based on the TERS image due to its spectral fingerprint. Only the combination of the two techniques (STM and TERS) allowed this conclusion.

Looking at the TERS images in Figure 5, the broad signal at 675 cm^{-1} observed in the spectrum next to the nanotape is the dominating TER signal within regions where nanotapes are absent. By using this mode as a marker band, the color-coded image in Figure 5c was obtained. It is clearly shown that a "negative" of the nanotape TERS image in Figure 5b is obtained. Therefore, we concluded that the substance causing this broad band (that can also be seen in the brown spectra in Figure 3) seems to cover the empty Au surface. We tentatively assume that it originates from the ambient environment (possibly from air) and settles down on the surface after the sample preparation or may stem from the sample preparation itself. In any case, this did not influence our imaging experiments. Note that the observation of this substance was only possible due to the full spectroscopic imaging that allowed post measurement data analysis.
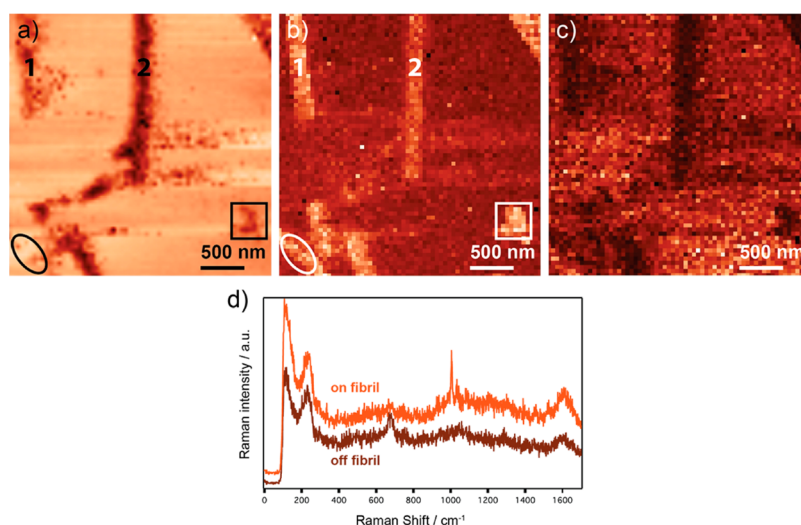
Figure 5. Simultaneously acquired (a) STM and (b,c) TERS (acquisition time 1 s/pixel, 2 mW incident power) images of individual nanotapes with $3 \times 3 \ \mu m^2$ scan size and 64×64 pixel resolution. The color-coded TERS images display (b) the intensity of the aromatic ring breathing marker band ($1004 \ cm^{-1}$, value of the peak integral) and (c) the band at $675 \ cm^{-1}$ that can be seen in the brown spectrum in (d). (d) Representative TER spectra taken from the full spectrum map that the TER images in (b,c) are based on. Nanotapes 1 and 2 and the circle and square highlight the different STM contrasts and TERS intensities in each region, strongly giving evidence of observed structural and/or chemical heterogeneity between the nanostructures.

Additionally, this feature would not have been observed by the STM measurement alone as this substance did not cause any contrast in the STM signal and the chemical information derived from the full spectroscopic imaging was missing.

The lateral resolution achieved was determined from the spectroscopic image by plotting the marker band intensity across a nanotape from a higher resolution image obtained with the same tip (64×64 pixel resolution with $1 \times 1 \ \mu m^2$ scan size, acquisition time 1 s/pixel, 2 mW incident laser power) against the scanned distance. A Gaussian fit resulted in a full width at half-maximum (fwhm) value of 78 nm for the nanotape width (see Figures S5 and S6 in the Supporting Information), which is a somewhat poor resolution for TERS (a spatial resolution down to <15 nm has been shown by Georgi et al.)[50,51] but still well below the optical diffraction limit. Note that, compared to the estimated width of the nanotapes from the AFM images (around 200 nm), 78 nm is a very small value for the fwhm of a nanotape. However, in the STM experiment, a broad tip is moving *down* when reaching a nanotape, whereas in the AFM experiment, a sharp tip is moving *up* when crossing a nanotape. It was not the aim of this study to achieve the highest possible spatial resolution but rather to simultaneously record STM and TERS images of a very weak biological Raman scatterer based on reproducible spectra in the fingerprint region. To our knowledge, the images shown are the first TERS images of this kind. The subdiffraction chemical information deduced from the corresponding TER spectrum can be directly correlated to the topographic information obtained from the corresponding STM image.

CONCLUSIONS AND OUTLOOK

This study shows that reproducible fingerprint TER spectra of a weakly scattering biological sample can be measured and used to generate TERS images that match the simultaneously obtained STM images. The TERS images deliver additional spectroscopic information. The data evaluation used to generate the TERS images were done in an automated and unbiased way, rather than relying on the individual assignment of spectra hand-picked by the researcher. The Ac-16–22-NH_2 β-amyloid(1–40) peptide fragment was used to prepare a submonolayer sample of amyloid nanotapes on an ultraflat Au substrate. AFM imaging and cross section analyses revealed that they are 5.4 ± 0.9 nm in height, 203.7 ± 18.0 nm in width, and several micrometers in length. These dimensions together with the FTIR and bulk confocal Raman data imply that the nanotapes consist of peptide bilayers with β-sheet structure. We demonstrated that the TERS spectra closely matched the bulk confocal Raman spectra for the sample. Simultaneously obtained gap-mode STM-TERS and STM images of individual nanotapes were presented in which full spectroscopic information was obtained in every pixel that provided the opportunity to choose spectral features of interest. The intensity of a marker band in the Raman fingerprint region (aromatic ring breathing mode) of the nanotapes was used to generate images that match the observed STM topography. The spatial resolution of the spectroscopic image was less than 78 nm—well below the optical diffraction limit. The nanotape dimensions obtained by the TER and STM images also correlate to the ones from the AFM images of the same sample. It is shown that

the spectral fingerprint pattern of the TER spectrum in the full spectral map, the TER point spectrum recorded for a longer time, and the bulk confocal Raman spectrum of the nanotapes correlate well, which assures comparability and allows one to exclude contamination. By comparing the STM and the TERS images, it was shown that topographic and chemical/spectroscopic information collected simultaneously allowed one to observe nanotapes that are not visible in the STM image, to find a difference between the signal intensity and the height information, to identify the coverage of the surface with an unknown substance, and to assign structure to a protein assembly that could not be unambiguously assigned by using STM imaging alone. A second full spectrum TER map of the nanotapes

collected on a different spot on the sample confirms the reproducibility of our experiment.

Overall, this study proves the potential of TERS as a reliable method that yields reproducible spectra and provides new insights into nanoscale biological samples that would not have been possible with other methods. In the future, TERS could be used to study more complex samples consisting of multicomponent biological specimens or complex materials that cannot be analyzed based on scanning probe microscopy alone. Samples such as native biological membranes, polymer interfaces, or nanofabricated devices could be investigated. We are confident that TERS will eventually become a valuable routine technique for the nanoscale characterization of surfaces.

METHODS

AFM Measurements. The AFM measurements were performed on a commercial AFM system (BioScope Catalyst, Bruker Nano, Santa Barbara, California) that is mounted onto an inverted confocal laser-scanning microscope (FluoView FV500, Olympus, Center Valley, Pennsylvania). The images shown in this study were obtained using tapping mode AFM with ATEC NC cantilever probes (Nanosensors, Neuchatel, Switzerland). The images (Figure 1, left to right) are 10, 3, and 1 μm in size, with a resolution of 256×256 pixels, and a scan rate of 1 Hz used.

TERS Setup. The commercial AFM/STM Raman microscope (NTEGRA Spectra Upright, NT-MDT, Moscow, Russia) used in this study was already described in detail by Stadler et al.[52] A HeNe laser with an excitation wavelength of 632.8 nm was applied. For the TERS images (and the confocal control) shown in this study, a laser power of 2 mW and an acquisition time for each pixel of 1 s was used. For the stronger TERS measurement shown in Figure 3, the laser power was adjusted with the help of neutral density filters to 240 μW, and the acquisition time increased to 2 min. The laser power was reduced for the longer measurement to avoid sample decomposition due to laser-induced heating. The confocal Raman spectrum of bulk nanotapes was acquired for 30 min with a laser power of 2 mW. Full metal Ag tips in STM feedback with a template-stripped Au substrate are used in this study; therefore, this kind of TERS measurement is commonly referred to as gap-mode STM-TERS.

To ensure that the TERS imaging is reproducible, several spots on the sample with different individual nanotapes were scanned. The corresponding images can be seen in Figure 4 and Figure 5 (also in Figure S5 of the Supporting Information). Additionally, the TER spectra were compared with the confocal bulk Raman spectrum of the nanotapes in order to ascertain that the observed TER spectral fingerprint matches the confocal Raman spectrum and that random parasitic persistent contaminations are not measured (see Figure 3). A confocal Raman control measurement of the sample (with the same laser power and integration time/pixel) can be seen in Figure S3 in the Supporting Information.

TERS Tips. The TERS tips used in this study were electrochemically etched from silver wires (diameter 0.25 mm, 99.99% purity, Sigma Aldrich) in a 1:1 (v/v) mixture of perchloric acid (70%, VWR) and methanol (p.a., Sigma Aldrich) using a potential of 8 V. Subsequently, they were thoroughly rinsed with methanol and preselected with the help of a Nikon 360× stereomicroscope according to their sharpness. The tip was mounted into the STM tip holder and brought into STM feedback with the template-stripped Au substrate. The focused HeNe laser beam was scanned over the Ag tip, and spectra were collected for each pixel. This created a spectral intensity map to determine the most enhancing spot on the Ag tip. After this determination, the HeNe laser was guided and focused to that spot. For the

TERS measurements, the laser was fixed into this position, and the sample was moved by the means of a XYZ piezo scanning stage.

Samples. *Peptide Synthesis and Aβ(16–22) Solution Preparation.* The lyophilized Ac-16–22-NH$_2$ peptide (sequence: N-acetyl-KLVFFAE-NH$_2$) was synthesized (CanPeptide, Ottawa, Canada), and N-terminal acetylation and C-terminal amidation were performed. The peptide was purified (>95%) by RP HPLC and finally characterized using MALDI-TOF mass spectrometry. The samples utilized for the far-field and near-field measurements were prepared by initially dissolving 3.57 mg of peptide in 0.1 mM deuterium chloride (Cambridge Isotope Laboratories, Andover, Massachusetts) and waiting for 5–6 h. No effect on nanotape formation could be observed if using deuterium chloride instead of hydrogen chloride. The solution was lyophilized overnight (Modulyod freeze-dryer, ThermoElectron Inc., Milford, Massachusetts) and stored at −20 °C until use. A 2 mM peptide solution was made by dissolving the lyophilized powder in 2 mL of deuterium oxide (Sigma Aldrich), vortexed to mix, and incubated at room temperature until further use.

Sample Substrates. The template-stripped Au substrates that were used in the gap-mode STM-TERS experiments were produced as described previously by Blum et al.[31]

Piranha cleaned (H$_2$SO$_4$/H$_2$O$_2$, 3:1, v/v) glass coverslips were thoroughly rinsed with ultrapure water (NANOpure Diamond, 18.2 MΩ·cm) and ethanol (Scharlau S.L.), subsequently dried in a stream of nitrogen gas, and directly used for the confocal Raman measurements.

TERS Sample Preparation. Forty microliters of the vortexed, deuterated Aβ(16–22) solution aged for approximately 2 weeks at room temperature was deposited on a freshly template-stripped Au substrate for approximately 5 min. It was briefly rinsed with a gentle stream of 18.2 MΩ·cm water and dried with flowing N$_2$ gas.

Sample Preparation for Confocal Raman Spectroscopy. The solvent for the Aβ(16–22) solution was removed by using a vacuum concentrator (Christ RVC 2-18, Martin Christ GmbH, Germany), set at room temperature, running for approximately 2.5 h until a dry powder was obtained. The powder was placed on an ethanol-rinsed, N$_2$-dried glass slide, compressed into a small pellet using a spatula and placed on the stage in the TERS instrument.

Sample Preparation for FTIR Spectroscopy. Approximately 20 μL of the aged and concentrated Aβ(16–22) nanotape solution was deposited between two CaF$_2$ windows and placed in an IR sample holder. Thirty-two scans were obtained and averaged (Perkin-Elmer, Spectrum 100 Optica). The spectrum of a D$_2$O background was subtracted from the sample spectra.

Data Processing. For the spectra shown, neither a background correction nor smoothing was performed to ensure comparability. The spectra were offset in the y-axis for better visibility. The stronger TER spectrum (green) and the bulk confocal

Raman spectrum (gray) in Figure 3 were multiplied in the *y*-axis (factor 0.3 and 0.02) to display them in the same graph as the other spectra. The processing of the TERS imaging data was performed with the associated software of the instrument, and the resulting images were exported as .jpg. For the Raman images in Figures 3b and 4b, the area under the peak at 1004 cm^{-1} (aromatic ring breathing mode) with respect to the surrounding background was calculated and plotted color-coded. The Raman image in Figure 4c shows the peak maximum with respect to the surrounding background in the same color-coded way (brighter pixel represents higher peak value). The STM images were linewise slope corrected.

Conflict of Interest: The authors declare no competing financial interest.

Supporting Information Available: Two figures showing the width and height analysis of the individual nanotapes, a figure showing the confocal control measurement, an IR spectrum of the nanotapes, the evaluation of the spatial resolution, and a table of the band assignment of the bulk confocal Raman spectrum are provided. This material is available free of charge *via* the Internet at http://pubs.acs.org.

REFERENCES AND NOTES

1. Pettinger, B.; Schambach, P.; Villagómez, C. J.; Scott, N. Tip-Enhanced Raman Spectroscopy: Near-Fields Acting on a Few Molecules. *Annu. Rev. Phys. Chem.* **2012**, *63*, 17.1–17.21.
2. Novotny, L.; Hecht, B. *Principles of Nano-Optics*; Cambridge University Press: Cambridge, 2006.
3. Stadler, J.; Schmid, T.; Zenobi, R. Developments in and Practical Guidelines for Tip-Enhanced Raman Spectroscopy. *Nanoscale* **2012**, *4*, 1856–1870.
4. Schmid, T.; Messmer, A.; Yeo, B.-S.; Zhang, W.; Zenobi, R. Towards Chemical Analysis of Nanostructures in Biofilms II: Tip-Enhanced Raman Spectroscopy of Alginates. *Anal. Bioanal. Chem.* **2008**, *391*, 1907–1916.
5. Domke, K. F.; Pettinger, B. Studying Surface Chemistry beyond the Diffraction Limit: 10 Years of TERS. *Chem. Phys. Chem.* **2010**, *11*, 1365–1373.
6. Ringler, P.; Schulz, G. E. Self-Assembly of Proteins into Designed Networks. *Science* **2003**, *302*, 106–109.
7. Zhang, S.; Marini, D. M.; Hwang, W.; Santoso, S. Design of Nanostructured Biological Materials through Self-Assembly of Peptides and Proteins. *Curr. Opin. Chem. Biol.* **2002**, *6*, 865–871.
8. Hartgerink, J. D.; Beniash, E.; Stupp, S. I. Self-Assembly and Mineralization of Peptide-Amphiphile Nanofibers. *Science* **2001**, *294*, 1684–1688.
9. Gazit, E. Self-Assembled Peptide Nanostructures: The Design of Molecular Building Blocks and Their Technological Utilization. *Chem. Soc. Rev.* **2007**, *36*, 1263–1269.
10. Cui, H.; Muraoka, T.; Cheetham, A. G.; Stupp, S. I. Self-Assembly of Giant Peptide Nanobelts. *Nano Lett.* **2009**, *9*, 945–951.
11. Burkoth, T. S.; Benzinger, T. L. S.; Urban, V.; Morgan, D. M.; Gregory, D. M.; Thiyagarajan, P.; Botto, R. E.; Meredith, S. C.; Lynn, D. G. Structure of the Beta-Amyloid(10−35) Fibril. *J. Am. Chem. Soc.* **2000**, *122*, 7883–7889.
12. Kirschner, D. A.; Inouye, H.; Duffy, L. K.; Sinclair, A.; Lind, M.; Selkoe, D. J. Synthetic Peptide Homologous to Beta Protein from Alzheimer Disease Forms Amyloid-like Fibrils *in Vitro*. *Proc. Natl. Acad. Sci. U.S.A.* **1987**, *84*, 6953–6957.
13. Krysmann, M. J.; Castelletto, V.; Kelarakis, A.; Hamley, I. W.; Hule, R. A.; Pochan, D. J. Self-Assembly and Hydrogelation of an Amyloid Peptide Fragment. *Biochemistry* **2008**, *47*, 4597–4605.
14. Hilbich, C.; Kisters-Woike, B.; Reed, J.; Masters, C. L.; Beyreuther, K. Substitutions of Hydrophobic Amino Acids Reduce the Amyloidogenicity of Alzheimer's Disease βA4 Peptides. *J. Mol. Biol.* **1992**, *228*, 460–473.
15. Balbach, J. J.; Ishii, Y.; Antzutkin, O. N.; Leapman, R. D.; Rizzo, N. W.; Dyda, F.; Reed, J.; Tycko, R. Amyloid Fibril Formation by Aβ16−22, a Seven-Residue Fragment of the Alzheimer's β-Amyloid Peptide, and Structural Characterization by Solid State NMR. *Biochemistry* **2000**, *39*, 13748–13759.
16. Senguen, F. T.; Doran, T. M.; Anderson, E. A.; Nilsson, B. L. Clarifying the Influence of Core Amino Acid Hydrophobicity, Secondary Structure Propensity, and Molecular Volume on Amyloid-B 16−22 Self-Assembly. *Mol. BioSyst.* **2011**, *7*, 497–510.
17. Whitesides, G. M.; Grzybowski, B. Self-Assembly at All Scales. *Science* **2002**, *295*, 2418–2421.
18. Gordon, D. J.; Balbach, J. J.; Tycko, R.; Meredith, S. C. Increasing the Amphiphilicity of an Amyloidogenic Peptide Changes the β-Sheet Structure in the Fibrils from Antiparallel to Parallel. *Biophys. J.* **2004**, *86*, 428–434.
19. Tao, K.; Wang, J.; Zhou, P.; Wang, C.; Xu, H.; Zhao, X.; Lu, J. R. Self-Assembly of Short Aβ(16−22) Peptides: Effect of Terminal Capping and the Role of Electrostatic Interaction. *Langmuir* **2011**, *27*, 2723–2730.
20. Mehta, A. K. A.; Lu, K. K.; Childers, W. S. W.; Liang, Y. Y.; Dublin, S. N. S.; Dong, J. J.; Snyder, J. P. J.; Pingali, S. V. S.; Thiyagarajan, P. P.; Lynn, D. G. D. Facial Symmetry in Protein Self-Assembly. *J. Am. Chem. Soc.* **2008**, *130*, 9829–9835.
21. Petty, S. A.; Decatur, S. M. Experimental Evidence for the Reorganization of β-Strands within Aggregates of the Aβ-(16−22) Peptide. *J. Am. Chem. Soc.* **2005**, *127*, 13488–13489.
22. Opilik, L.; Bauer, T.; Schmid, T.; Stadler, J.; Zenobi, R. Nanoscale Chemical Imaging of Segregated Lipid Domains Using Tip-Enhanced Raman Spectroscopy. *Phys. Chem. Chem. Phys.* **2011**, *13*, 9978–9981.
23. Carrier, S. L.; Kownacki, C. M.; Schultz, Z. D. Protein−Ligand Binding Investigated by a Single Nanoparticle TERS Approach. *Chem. Commun.* **2011**, *47*, 2065–2067.
24. Domke, K. F.; Zhang, D.; Pettinger, B. Tip-Enhanced Raman Spectra of Picomole Quantities of DNA Nucleobases at Au(111). *J. Am. Chem. Soc.* **2007**, *129*, 6708–6709.
25. Hennemann, L. E.; Meixner, A. J.; Zhang, D. Surface- and Tip-Enhanced Raman Spectroscopy of DNA. *Spectroscopy* **2010**, *24*, 119–124.
26. Hermann, P.; Fabian, H.; Naumann, D.; Hermelink, A. Comparative Study of Far-Field and Near-Field Raman Spectra from Silicon-Based Samples and Biological Nanostructures. *J. Phys. Chem. C* **2011**, 24512–24520.
27. Gullekson, C.; Lucas, L.; Hewitt, K.; Kreplak, L. Surface-Sensitive Raman Spectroscopy of Collagen I Fibrils. *Biophys. J.* **2011**, *100*, 1837–1845.
28. Moretti, M.; Proietti Zaccaria, R.; Descrovi, E.; Das, G.; Leoncini, M.; Liberale, C.; De Angelis, F.; Di Fabrizio, E. Reflection-Mode TERS on Insulin Amyloid Fibrils with Top-Visual AFM Probes. *Plasmonics* **2012**, 10.1007/s11468-012-9385-x.
29. Kurouski, D.; Deckert-Gaudig, T.; Deckert, V. Structure and Composition of Insulin Fibril Surfaces Probed by TERS. *J. Am. Chem. Soc.* **2012**, *134*, 13323.
30. Blum, C.; Schmid, T.; Opilik, L.; Metanis, N.; Weidmann, S.; Zenobi, R. Missing Amide I Mode in Gap-Mode Tip-Enhanced Raman Spectra of Proteins. *J. Phys. Chem. C* **2012**, *116*, 23061–23066.
31. Blum, C.; Schmid, T.; Opilik, L.; Weidmann, S.; Fagerer, S. R.; Zenobi, R. Understanding Tip-Enhanced Raman Spectra of Biological Molecules: A Combined Raman, SERS and TERS Study. *J. Raman Spectrosc.* **2012**, 10.1002/jrs.4099.
32. Yokoi, H.; Kinoshita, T.; Zhang, S. Dynamic Reassembly of Peptide RADA16 Nanofiber Scaffold. *Proc. Natl. Acad. Sci. U.S.A.* **2005**, *102*, 8414–8419.
33. Dong, H.; Paramonov, S. E.; Aulisa, L.; Bakota, E. L.; Hartgerink, J. D. Self-Assembly of Multidomain Peptides: Balancing Molecular Frustration Controls Conformation and Nanostructure. *J. Am. Chem. Soc.* **2007**, *129*, 12468–12472.

34. Nyrkova, I. A.; Semenov, A. N.; Aggeli, A.; Boden, N. Fibril Stability in Solutions of Twisted-Sheet Peptides: A New Kind of Micellization in Chiral Systems. *Eur. Phys. J. B* **2000**, *17*, 481–497.

35. Chirgadze, Y. N.; Nevskaya, N. A. Infrared Spectra and Resonance Interaction of Amide-I Vibration of the Anti-parallel-Chain Pleated Sheet. *Biopolymers* **1976**, *15*, 607–625.

36. Apetri, M. M.; Maiti, N. C.; Zagorski, M. G.; Carey, P. R.; Anderson, V. E. Secondary Structure of α-Synuclein Oligomers: Characterization by Raman and Atomic Force Microscopy. *J. Mol. Biol.* **2006**, *355*, 63–71.

37. Schmid, T.; Sebesta, A.; Stadler, J.; Opilik, L.; Balabin, R. M.; Zenobi, R. Tip-Enhanced Raman Spectroscopy and Related Techniques in Studies of Biological Materials. *Proc. SPIE* **2010**, *7586*, 758603.1−13.

38. Stewart, S.; Fredericks, P. Surface-Enhanced Raman Spectroscopy of Amino Acids Adsorbed on an Electrochemically Prepared Silver Surface. *Spectrochim. Acta, Part A* **1999**, *55*, 1641–1660.

39. Guicheteau, J.; Argue, L.; Hyre, A.; Jacobson, M.; Christesen, S. D. Raman and Surface-Enhanced Raman Spectroscopy of Amino Acids and Nucleotide Bases for Target Bacterial Vibrational Mode Identification. *SPIE* **2006**, *6218*, 62180O.1−11.

40. Kim, S. K.; Kim, M. S.; Suh, S. W. Surface-Enhanced Raman-Scattering (SERS) of Aromatic-Amino-Acids and Their Glycyl Dipeptides in Silver Sol. *J. Raman Spectrosc.* **1987**, *18*, 171–175.

41. Podstawka, E.; Ozaki, Y.; Proniewicz, L. Part I: Surface-Enhanced Raman Spectroscopy Investigation of Amino Acids and Their Homodipeptides Adsorbed on Colloidal Silver. *Appl. Spectrosc.* **2004**, *58*, 570–580.

42. Herne, T. M.; Ahern, A.; Garrell, R. L. Surface-Enhanced Raman Spectroscopy of Peptides: Preferential N-Terminal Adsorption on Colloidal Silver. *J. Am. Chem. Soc.* **1991**, *113*, 846–854.

43. Huang, C.-Y.; Balakrishnan, G.; Spiro, T. G. Protein Secondary Structure From Deep-UV Resonance Raman Spectroscopy. *J. Raman Spectrosc.* **2006**, *37*, 277–282.

44. Bandekar, J. Amide Modes and Protein Conformation. *Biochim. Biophys. Acta* **1992**, *1120*, 123–143.

45. Stewart, S.; Fredericks, P. M. Surface-Enhanced Raman Spectroscopy of Peptides and Proteins Adsorbed on an Electrochemically Prepared Silver Surface. *Spectrochim. Acta, Part A* **1999**, *55*, 1615.

46. García, R.; Tamayo, J.; Bustamante, C. Scanning Tunneling Microscopy Imaging and Selective Modification of Purple Membranes. *Int. J. Imaging Syst. Technol.* **1997**, *8*, 168–174.

47. Nevernov, I.; Kurnikov, I.; Nicolini, C. Mechanical Interactions in STM Imaging of Large Insulating Adsorbates. *Ultramicroscopy* **1995**, *58*, 269–274.

48. Domke, K. F.; Zhang, D.; Pettinger, B. Enhanced Raman Spectroscopy: Single Molecules or Carbon? *J. Phys. Chem. C* **2007**, *111*, 8611–8616.

49. Pettinger, B.; Domke, K. F.; Zhang, D.; Picardi, G.; Schuster, R. Tip-Enhanced Raman Scattering: Influence of the Tip-Surface Geometry on Optical Resonance and Enhancement. *Surf. Sci.* **2009**, *603*, 1335–1341.

50. Georgi, C.; Hartschuh, A. Tip-Enhanced Raman Spectroscopic Imaging of Localized Defects in Carbon Nanotubes. *Appl. Phys. Lett.* **2010**, *97*, 143117.

51. Stadler, J.; Schmid, T.; Zenobi, R. Nanoscale Chemical Imaging of Single-Layer Graphene. *ACS Nano* **2011**, *5*, 8442–8448.

52. Stadler, J.; Schmid, T.; Zenobi, R. Nanoscale Chemical Imaging Using Top-Illumination Tip-Enhanced Raman Spectroscopy. *Nano Lett.* **2010**, *10*, 4514–4520.